Eichardt, Roland; Baumgarten, Daniel; Di Rienzo, Luca; Linzen, Sven; Schultze, Volkmar; Haueisen, Jens:

Localisation of buried ferromagnetic objects based on minimum-norm-estimations : a simulation study

URN: urn:nbn:de:gbv:ilm1-2014210082

Published OpenAccess: September 2014

Original published in:

Compel : international journal of computation & mathematics in electrical & electronic engineering. - Bradford : Emerald (ISSN-p 0332-1649). - 28 (2009) 5, S. 1327-1337.

DOI: 10.1108/03321640910969566

URL: http://dx.doi.org/10.1108/03321640910969566

[Visited: 2014-09-02]

COMPEL - The international journal for computation and ma... in electrical and electronic engineering

Localisation of buried ferromagnetic objects based on minimum-norm-estimations: A simulation study

Roland Eichardt Daniel Baumgarten Luca Di Rienzo Sven Linzen Volkmar Schultze Jens Haueisen

Localisation of buried ferromagnetic objects based on minimum-norm-estimations

A simulation study

Roland Eichardt
Institute for Biomedical Engineering and Informatics, Ilmenau University of Technology, Ilmenau, Germany

Daniel Baumgarten
Biomagnetic Center, Department of Neurology, University Hospital Jena, Jena, Germany

Luca Di Rienzo
Dipartimento di Elettrotecnica, Politecnico di Milano, Milano, Italy

Sven Linzen and Volkmar Schultze
Institute of Photonic Technology (IPHT), Jena, Germany, and

Jens Haueisen
Institute for Biomedical Engineering and Informatics, Ilmenau University of Technology, Ilmenau, Germany

Abstract

Purpose – The purpose of this paper is to examine the localisation of ferromagnetic objects buried in the underground. More specifically, it deals with the reconstruction of the XY-positions, the depths (Z-positions), the number, and the extension of the objects based on geomagnetic measurements. This paper introduces a minimum-norm reconstruction approach and evaluates its performance in a simulation study.

Design/methodology/approach – A minimum-L2-norm estimation based on the truncated singular value decomposition method with lead field weighting is proposed in order to localise geomagnetic sources. The sensor setup and positions are taken from real measurements. The source space is formed by an automatically generated grid. At each grid point, a magneto-static dipole is assumed.

Findings – Sources with different depths and XY-positions could be successfully reconstructed. The proposed approach is not overly sensitive to errors/noise in measurement values and sensor positions.

Originality/value – The approach described in this paper can be used for applications like geoprospection, archaeology, mine clearing, and the clean-up of former waste deposits.

Keywords Ferrous metals, Magnetism, Archaeology, Wastes, Localization

Paper type Research paper

This study was supported by the State of Thuringia/Germany (2006VF0011, 2008VF0001) under participation of the European Union within the European Funds for Regional Development and from the NATO Security through Science Programme PST.EAP.CLG.981130: "Detection of small metal objects by multi-component magnetic measurements." The authors thank the two anonymous reviewers for their helpful comments.

COMPEL: The International Journal for Computation and Mathematics in Electrical and Electronic Engineering
Vol. 28 No. 5, 2009
pp. 1327-1337

0332-1649
DOI 10.1108/03321640910969566

I. Introduction

The geomagnetic survey of the underground and the subsequent localisation of buried ferromagnetic objects or magnetic anomalies are of great interest in many fields, e.g. unexploded ordnance detection, archaeology, and building industry. Recently, such magnetic measurements have been performed with the help of detection systems using superconducting quantum interference device (SQUID) sensors (Linzen *et al.*, 2007). The advantage of SQUID-based measurements lays in its much higher sensitivity and dynamic range as compared to other commercially available sensor techniques. The high sensitivity is especially important for the localisation of small objects or the estimation of the extent of larger objects, which require a detailed magnetic field profile and, at the same time, a sufficiently high signal-to-noise ratio (SNR). In realistic situations of geomagnetic surveys, extended sources or multiple close-by sources occur often. Archaeologists for instance are interested in extended buried structures on the base of the generated geo-referenced magnetic maps (Linzen *et al.*, 2007; Schultze *et al.*, 2008).

For the localisation of buried ferromagnetic objects based on the measured magnetic field distribution, non-linear search methods from Levenberg-Marquardt and Powell were used before (McFee *et al.*, 1990; Barrel and Naus, 2007). In Munschy *et al.* (2007), a magnetic mapping approach was used to detect unexploded ordnance in the ground. Typically, such localisation methods have advantages when only one focal source is to be reconstructed. In case of multiple, distributed, or extended sources, non-linear search methods are difficult to apply. Thus, in the case of real data, where the number and the extent of sources are not known a-priori, linear estimation techniques like the minimum-L2-norm method might prove useful. Therefore, the aim of our study is to introduce a minimum-norm approach to the reconstruction of geomagnetic sources. In this first simulation study, we examine the performance of our approach on selected simple source configurations. More specifically, we use a real measurement setup from measurements of buried ferromagnetic objects and quantify by means of repeated simulations the influence of noise and the effects of different reconstruction grids on the inverse solution.

II. Methods

Sensor setup

The simulations base on experimental data which were recorded by a low-temperature SQUID measurement system (Linzen *et al.*, 2007). This device was developed at the Institute of Photonic Technology Jena in collaboration with the Supracon AG Jena. It utilises the high-magnetic field sensitivity and high bandwidth of SQUID sensors for large area geomagnetic surveying and mapping.

The system consists of a non-magnetic vehicle which carries up to three liquid helium filled cryostats, containing several SQUID sensors (Figure 1). During measurement, the magnetic signatures of buried objects and anomalies in the underground are sampled. An inertial system and a differential global positioning system provide precise positions and orientations of the SQUID sensors for each of the measurement samples. A recorded data set consists of successively scanned lines with measurement point distances of only a few centimetres and a line-to-line distance of about half-a-metre.

Notes: The vehicle can carry up to three helium cryostats - here a two channel configuration is shown

Figure 1.
The SQUID measurement system in action

Each measurement channel of the system is represented by at least one highly balanced planar SQUID gradiometer of first order and a SQUID magnetometer triplet (Figure 2). The highly balanced gradiometers are the base for the required magnetically unshielded operation of the system under earth field conditions. The gradiometers inside the cryostats are oriented to detect the $dB_{horizontal}/dz$ components of the magnetic field gradient tensor, where z is the vertical direction.

The sensor setup we use for the simulations shown in this paper is taken from a real measurement using one gradiometer channel. It includes 4,862 sensor positions and orientations in an area of 10 m × 10 m (Figure 3).

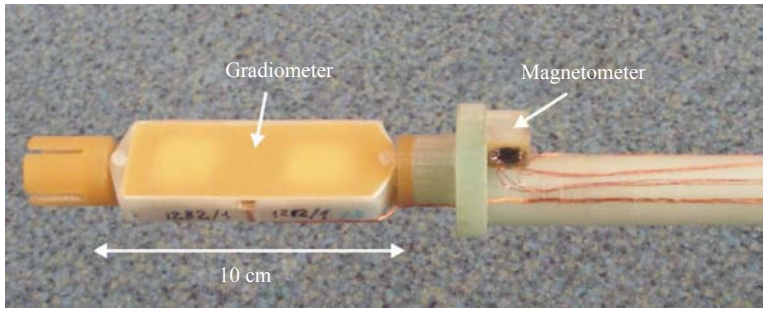

Notes: The bundled copper wires in the upper part lead to the readout electronics on top of the cryostat

Figure 2.
Photograph of a cryostat inset holding one SQUID gradiometer and a SQUID magnetometer triple

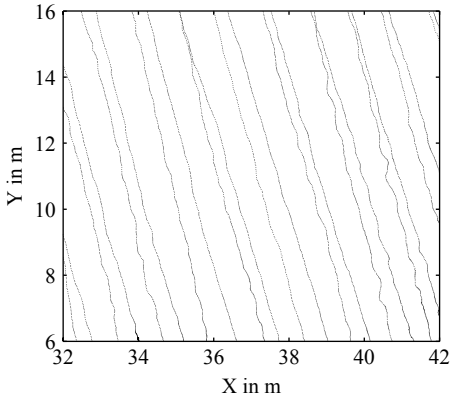

Figure 3.
Sensor positions derived from a real measurement (4,862 measurement points, ·) that are used in the simulations

Forward model

The source space for the minimum-norm-estimation is formed by an automatically generated regular grid below the measurement area. The distance of grid points in X, Y, and Z direction, and the maximum depths of the grid are defined by parameters shown in Table I. At each grid point, a dipole is defined as source, since with a combination of dipoles any given source can be approximated. Since the magnetic field can be considered static and the relative magnetic permeability of the underground can be approximated homogeneously with $\mu_r \approx 1$, we use the magneto-static dipole to model the sources at the grid points. The magnetic field $\vec{B}$ at position $\vec{r}$ that is produced by a magnetic dipole at position $\vec{r}'$ with moment $\vec{m}$ (μ_0 is the permeability of free space) is computed according to:

$$\vec{B}(\vec{r}) = \frac{\mu_0}{4\pi}\left(\frac{3\vec{m}\cdot(\vec{r}-\vec{r}\,')}{|\vec{r}-\vec{r}\,'|^5}(\vec{r}-\vec{r}\,') - \frac{\vec{m}}{|\vec{r}-\vec{r}\,'|^3}\right) \quad (1)$$

Inverse method

For the localisation of ferromagnetic objects and magnetic anomalies in the underground, a minimum-norm-estimation (Wang *et al.*, 1993; Hämäläinen *et al.*, 1993) using the truncated singular value decomposition (TSVD) method (Hansen, 1997) is applied. The forward model containing information on sensor positions and orientations as well as on the grid sources is represented in the lead field matrix $\mathbf{L}$. An estimation for the source activity vector $\mathbf{m}_r$, which describes the magnitudes of the

Simulation no.	Source no.	SNR level(s) in dBA	Repeated runs in no.	Grid point distance in m	Grid depth in m	Reg. parameter σ_r
1	1, 2, 3	15	10	0.75	−2.45	0.01
2	2	2.5, 5, 7.5, 10, 15, ∞	20	0.75	−2.45	0.01, 0.02, 0.03
3	4	15	10	0.75	−2.45	0.02
4	2, 5	15	10	1.0, 0.75, 0.5	−1.75, −2.5, −3.25	0.02
5	4	15	10	0.75	−2.45	0.02

Table I.
Parameters for the simulation runs

dipoles in the grid, can be obtained by multiplying the pseudo inverse of the lead field matrix $\mathbf{L}_r^+$ with the measurement value vector $\mathbf{b}$ by using the TSVD of $\mathbf{L}$ as shown in equation (2). The rank r of $\mathbf{L}_r^+$ is determined by the index i of the smallest singular value σ_i in the sorted sequence $\Sigma = diag(\sigma_1, \ldots, \sigma_n)$ that is equal to or greater than the regularisation parameter σ_r:

$$\mathbf{m}_r = \mathbf{L}_r^+ \cdot \mathbf{b} = (\mathbf{U}\Sigma\mathbf{V}^T)_r^+ \cdot \mathbf{b} = \sum_{i=0}^{r} \frac{\mathbf{u}_i^T \mathbf{b}}{\sigma_i} \mathbf{v}_i \tag{2}$$

To compensate the preference of the minimum-norm-estimation for superficial sources, we incorporated a lead field weighting into the TSVD by using the diagonal weighting matrix $\mathbf{W}$ defined in equation (3), whereas $\|\mathbf{l}_i\|$ is the Euclidean norm of the ith column of $\mathbf{L}$:

$$\mathbf{W} = \mathrm{diag}\left(\frac{1}{\|\mathbf{l}_i\|}\right). \tag{3}$$

The weighted minimum-norm solution is derived from equation (2) with the singular value decomposition of $\mathbf{LW} = \mathbf{U}'\Sigma'\mathbf{V}'^T$ (Jeffs *et al.*, 1987; Phillips *et al.*, 1997), as follows:

$$\mathbf{m}'_r = \mathbf{W}(\mathbf{LW})_r^+ \cdot \mathbf{b} = \mathbf{W}(\mathbf{U}'\Sigma'\mathbf{V}'^T)_r^+ \cdot \mathbf{b} = \mathbf{W}\sum_{i=0}^{r} \frac{\mathbf{u}_i'^T \mathbf{b}}{\sigma_i'} \mathbf{v}'_i. \tag{4}$$

By analyzing the estimated distribution of the activities of the grid sources $\mathbf{m}$, the location of a dipolar source is determined by using the coordinates of the strongest dipole in an area of activation.

Simulations

To evaluate the performance of the proposed inverse method in the reconstruction of geomagnetic measurements, we perform several simulations with parameters shown in Table I for the dipolar sources defined in Table II. By means of these simulations, we study the influence of the following parameters on the inverse solution:

- depth of sources (Z-position);
- added white Gaussian noise and regularisation parameters σ_r;
- different XY-positions in a three-dipole simulation;
- grid parameters (grid depth and distance of points); and
- errors in the sensor positions and orientations.

Source configuration no.	Used in simulation(s)	Dipole positions (X, Y, Z) in m	Moment in Am^2
1	1	(37.25, 11.25, −0.75)	$(0, 0, 1 \times 10^{-6})$
2	1, 2, 4	(37.25, 11.25, −1.45)	$(0, 0, 1 \times 10^{-6})$
3	1	(37.25, 11.25, −2.15)	$(0, 0, 1 \times 10^{-6})$
4.1	3, 5	(38.75, 11.25, −0.75)	$(0, 0, 1.0 \times 10^{-6})$
4.2		(35.25, 8.75, −0.75)	$(0, 0, 0.9 \times 10^{-6})$
4.3		(35.25, 13.25, −0.75)	$(0, 0, 1.1 \times 10^{-6})$
5	4	(38.75, 9.75, −1.4)	$(0, 0, 1 \times 10^{-6})$

Table II. Source parameters used in the dipole simulations

The gradiometer data at the sensor positions (shown in Figure 3) are simulated using the magnetostatic sources specified in Table II. White Gaussian noise with different SNR is added, and repeated simulation runs with different noise realisations are conducted. To evaluate the quality of the inverse solution and to measure the localisation error, we use the Euclidean distance d_{Opt} between the real position of the source in Table II (optimum) and the position of the estimated grid dipole with maximum reconstructed magnitude. To evaluate simulations with $n = 3$ simultaneous sources, the reconstructed dipole distribution is clustered in three regions with:

(1) $X \geq 37.25$ m;

(2) $X < 37.25$ m and $Y < 11$ m; and

(3) $X < 37.25$ m and $Y \geq 11$ m.

For each region with index i, the distance d^i_{opt} to the simulated source in this region is calculated; the overall distance is defined by:

$$d_{opt} = \frac{1}{n}\sum_{i=1}^{n} d^i_{opt}.$$

III. Results

The five simulations described in the previous paragraph lead to the following results:

(1) *Simulation 1.* The condition number of the lead field matrices is relatively large with a value of $1.48 \times 10^{+16}$, which implies a considerably ill-posed inverse problem. The inverse problems in Simulations 2, 3, and 5 exhibit a similarly high-condition number.

Table III contains the results for the three single dipoles located in different depths (for detailed parameters, see Tables I and II). The distance to the optimal dipole (d_{Opt}) is slightly higher for the deep source 3. When considering the positions of the grid points, the closest possible grid point is provided for the simulation sources 1 and 2 as result of the minimum-norm-estimation. For source 3, d_{Opt} is still clearly smaller than the space between the grid points (0.75 m). Figure 4 shows as an example two plots of the estimated dipole reconstruction in one X- and one Z-plane, which are proximate to the real position of the simulated source 2. Please note that the position of the dipolar source in the forward simulation was not on the reconstruction grid.

(2) *Simulation 2.* Figure 5(a) shows the average values for d_{Opt} using different levels of noise and regularisation parameters σ_r. The regularisation parameter $\sigma_r = 0.03$ produces results with larger distances from the optimum when the

Source no.	Source depth in m	Avg. reconstructed position (X, Y, Z) in m	Avg. d_{Opt} in m
1	−0.75	(37.5, 11.25, −0.95)	0.3302
2	−1.45	(37.25, 11.25, −1.7)	0.3536
3	−2.15	(36.75, 11.25, −2.45)	0.5831

Table III. Reconstruction results for the three sources in Simulation 1, each averaged over ten runs

Notes: All runs using different noise realisations lead to identical results. A regularisation parameter of $\sigma_r = 0.01$ is used

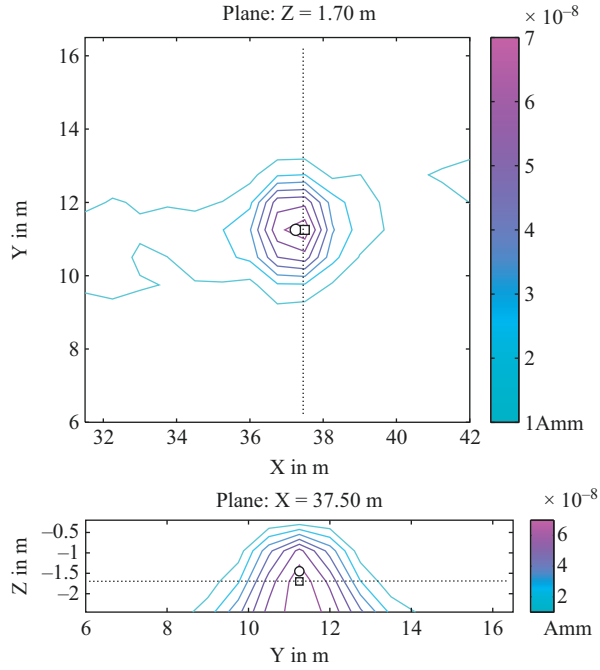

Notes: The estimated source position (marked with □) is in both planes proximate to the real position of source 2 indicated by ○

Figure 4.
Results of the minimum-norm-estimation in Simulation 2 for the planes of the regular grid of Z = −1.7 m (top) and X = 37.5 m (bottom)

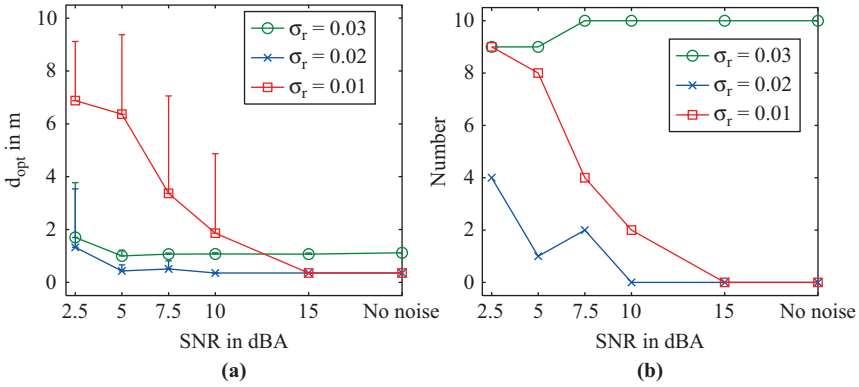

Notes: (a) Averaged values (marker: ○,□ and ×) and positive part of the standard deviation (vertical bars) of the localisation errors (d_{Opt}) for simulation 2 using different noise levels (SNR) and truncation thresholds (σ_r). (b) Number of runs (out of 10 noise realisations) with $d_{Opt} > 0.75$ m (space between grid points) for simulation 2 using different noise levels (SNR) and truncation thresholds (σ_r)

Figure 5.

noise level is low (SNR $\geq$ 15 dBA), but it is relatively insensitive to higher levels of noise. The best results for all tested SNRs using source 2 are obtained with $\sigma_r = 0.02$. With $\sigma_r = 0.01$ the results are also very good for SNR $\geq$ 15 dBA, but for increasing levels of noise the average distances of the results to the optimum are getting larger.

The evaluation in Figure 5(b) shows the number of runs (out of $n = 10$) with d_{Opt} larger than the space between the grid points which is 0.75 m. The results indicate a characteristic comparable to Figure 5(a). For all tested noise levels with $\sigma_r = 0.03$, nine and, respectively, ten results show $d_{Opt} > 0.75$ m. The performance of $\sigma_r = 0.02$ (for an SNR $\geq$ 10 dBA all runs have $d_{Opt} < 0.75$ m) is better than for $\sigma_r = 0.01$ ($d_{Opt} < 0.75$ m for all levels of SNR $\geq$ 15 dBA), again.

(3) *Simulation 3.* In Table IV, the results for the simultaneous reconstruction of the three dipoles of source configuration 4 are shown. All of the ten runs with different instances of noise (SNR = 15 dBA) lead to the same source positions. The localisation errors are with $d^1_{Opt} \approx 0.54$ m, $d^{2,3}_{Opt} \approx 0.32$ m, and $d_{Opt} \approx 0.39$ m low with respect to the grid space of 0.75 m.

(4) *Simulation 4.* Table V shows the influence of using different grids for the minimum-norm-estimation. The runs using grid spaces of 1 and 0.75 m located

Table IV.
Results of the simultaneous reconstruction of three sources in Simulation 3 averaged over ten runs

Source no.	Sim. source position (X, Y, Z) in m	Avg. reconstructed position (X, Y, Z) in m	Avg. d^i_{Opt} in m	Avg. d_{Opt} in m
4.1	(38.75, 11.25, −0.75)	(38.25, 11.25, −0.95)	0.5385	0.3929
4.2	(35.25, 8.75, −0.75)	(35.25, 9.0, −0.95)	0.3202	
4.3	(35.25, 13.25, −0.75)	(35.25, 13.5, −0.95)	0.3202	

Notes: All runs using different noise realisations lead to identical results. A regularisation parameter of $\sigma_r = 0.02$ is used

Table V.
Reconstruction results of Simulation 4 using different grid point spacings for source 2 and 5

Space between grid points in m	Grid points in Z, max … min in m	Number of grid points	Reconstructed position (X, Y, Z) in m	d_{Opt} in m	CN
Results for source 2 at (37.25, 11.25, −1.45)					
1.0	−0.5 … −2.5	363	(37.0, 11.0, −1.5)	0.3571	$7.72 \times 10^{+9}$
0.75	−0.25 … −1.75	675	(37.25, 11.25, −1.7)	0.3905	$3.63 \times 10^{+12}$
	−0.25 … −2.5	900			$2.70 \times 10^{+16}$
	−0.25 … −3.25	1125			$2.81 \times 10^{+18}$
0.5	−0.5 … −2.5	2205	(37.0, 11.0, −2.5)	1.1079	$9.53 \times 10^{+18}$
Results for source 5 at (38.75, 9.75, −1.4)					
1.0	−0.5 … −2.5	363	(39.0, 10.0, −1.5)	0.3674	$7.72 \times 10^{+9}$
0.75	−0.25 … −1.75	675	(39.0, 9.75, −1.75)	0.4301	$3.63 \times 10^{+12}$
	−0.25 … −2.5	900			$2.70 \times 10^{+16}$
	−0.25 … −3.25	1125			$2.81 \times 10^{+18}$
0.5	−0.5 … −2.5	2205	(39.0, 10.0, −2.5)	1.1554	$9.53 \times 10^{+18}$

Note: A regularisation parameter of $\sigma_r = 0.02$ is used

the sources with an accuracy of $d_{Opt} \leq 0.43$ m. A relatively fine grid with spaces between neighbour points of 0.5 m does not lead to a proper localisation of the simulated source: while the XY-coordinates fit well to the source, the Z-position is projected to the lowest grid point. Larger ($\sigma_r = 0.03$) and smaller ($\sigma_r = 0.01$) regularisation parameters produce worse results. The condition number increases with the number of grid points from $7.72 \times 10^{+9}$ (363 points) to $9.53 \times 10^{+18}$ (2,205 points); hence the stability of the inverse problem degrades. Furthermore, the maximum depth (Z) of grid points used for the reconstruction seems not to have a large impact on the reconstruction result, as long as the Z-position of the source is covered by the grid.

(5) *Simulation 5.* As indicated by Table VI, the applied errors in the sensor positions and orientations, realized by random modifications with zero mean and standard deviations of 0.01 m (for the position) and 10° (for each of the three directions), do not have a noticeable impact on the reconstruction result. The results are identical to Simulation 3 (Table IV) which uses the same three sources, but without errors in sensor positions and orientations.

IV. Conclusion

The simulation results show that minimum-norm-estimations using the TSVD approach can be successfully applied to the localisation of geomagnetic anomalies. Simulated measurement data using dipolar sources with different depths, XY-positions, magnitudes, and also with multiple simultaneous sources could be processed with good localisation accuracy. White Gaussian noise with SNR $\geq$ 15 dBA does not affect the localisation result considerably. The minimum-norm method also tolerates some errors in the sensor positions and orientations.

The regularisation parameter σ_r has to be set accurately. In general, larger parameters are more suitable for higher levels of noise, while smaller parameters provide more reliable depth localisations. Furthermore, the source localisation in X- and Y-direction is noticeably more robust against noise and regularisation compared to the depth localisation (Z-direction).

The number of grid points which define the source space (dipoles to estimate) has impact on the localisation accuracy as well as on the computational costs for the inverse solution. With a high number of grid points (and hence of the parameters to estimate) also the condition number of the related lead field matrix increases, which leads to a more ill-conditioned inverse problem. This causes the poor performance of the 0.5 m grid in Simulation 4. Other regularisation parameters do not provide better reconstruction results in this case either.

Source no.	Sim. source position (X, Y, Z) in m	Avg. reconstructed position (X, Y, Z) in m	Avg. d^i_{Opt} in m	Avg. d_{Opt} in m
4.1	(38.75, 11.25, −0.75)	(38.25, 11.25, −0.95)	0.5385	0.3929
4.2	(35.25, 8.75, −0.75)	(35.25, 9, −0.95)	0.3202	
4.3	(35.05, 13.25, −0.75)	(35.25, 13.5, −0.95)	0.3202	

Notes: All runs using different noise realisations lead to identical results. Noise exists in measurement values, sensor positions and orientations. A regularisation parameter of $\sigma_r = 0.02$ is used

Table VI. Reconstruction results for the three sources (configuration 4) in Simulation 5 averaged over ten runs

In this study, we did not focus on special parameter selection methods for the regularisation. We basically used standard truncation parameters of $\sigma_r = 0.01$ or $\sigma_r = 0.02$ for the TSVD method. In addition, also smaller ($\sigma_r = 0.005$) and larger ($\sigma_r = 0.03$) parameters were tested. However, these values produce results with noticeable noise artefacts and regularisation errors, respectively.

For the dipole search in Barrel and Naus (2007), the non-linear methods from Nelder-Mead and Powell are applied to localize magnetic and ferromagnetic objects. The results also indicate that the magneto-static dipole model is relatively robust compared to the magnetic quadrupol. In the presence of high noise or weak source signals both dipole search methods show the tendency to diverge, if they are not initialised appropriately (e.g. with respect to the initial guess of the dipole search and the number of sources).

In contrast, for the minimum-norm-estimation the number of sources does not need to be known and specified in advance. Hence, this approach is advantageous when multiple sources prevail in a geomagnetic measurement.

Minimum-norm methods might also be used in combination with techniques that are used for detection and classification of unexploded ordnance like proposed in Collins *et al.* (2001), Billings (2004) and Billings *et al.* (2006). With minimum-norm-estimations a preliminary inspection of the underground can be easily conducted. This can be done without a-priory knowledge or special adaptations to the measurement data. Only the regularisation parameter might have to be adjusted, especially when the noise in the measurement data considerably differs to former source estimations. Subsequently, objects in the located areas of interest can be classified and localised with higher accuracy using more complex techniques.

In future work, we will further analyse the influence of sensor errors and deal with the estimation of extended sources. Progressing research will also include the analysis of real measurement data.

References

Barrel, Y. and Naus, H.W.L. (2007), "Detection and localisation of magnetic objects", *IET Science, Measurement and Technology*, Vol. 1 No. 5, pp. 245-54.

Billings, S.D. (2004), "Discrimination and classification of buried unexploded ordnance using magnetometry", *IEEE Transactions on Geoscience and Remote Sensing*, Vol. 42 No. 6, pp. 1241-51.

Billings, S.D., Pasion, C., Walker, S. and Beran, L. (2006), "Magnetic models of unexploded ordnance", *IEEE Transactions on Geoscience and Remote Sensing*, Vol. 44 No. 8, pp. 2115-24.

Collins, L.M., Yan, Z., Jing, L., Hua, W., Carin, L., Hart, S.J., Rose-Pehrsson, S.L., Nelson, H.J. and McDonald, J.R. (2001), "A comparison of the performance of statistical and fuzzy algorithms for unexploded ordnance detection", *IEEE Transactions on Fuzzy Systems*, Vol. 9 No. 1, pp. 17-30.

Hämäläinen, M.S., Hari, R., Ilmoniemi, R.J., Knuutila, J. and Lounasmaa, O.V. (1993), "Magnetoencephalography – theory, instrumentation, and applications to noninvasive studies of the working human brain", *Reviews of Modern Physics*, Vol. 65 No. 2, pp. 413-97.

Hansen, P.C. (1997), *Rank-deficient and Discrete Ill-posed Problems*, SIAM, Philadelphia, PA.

Jeffs, B., Leahy, R. and Singh, M. (1987), "An evaluation of methods for neuromagnetic image reconstruction", *IEEE Transactions on Biomedical Engineering*, Vol. 34 No. 9, pp. 713-23.

Linzen, S., Chwala, A., Schultze, V., Schulz, M., Schüler, T., Stolz, R., Bondarenko, N. and Meyer, H.-G. (2007), "A LTS-SQUID system for archaeological prospection and its practical test in Peru", *IEEE Transactions on Applied Superconductivity*, Vol. 17 No. 2, pp. 750-5.

McFee, J.E., Das, Y. and Ellingson, R.O. (1990), "Magnetic locating and identifying compact ferrous objects", *IEEE Transactions on Geoscience and Remote Sensing*, Vol. 28 No. 2, pp. 182-93.

Munschy, M., Boulanger, D., Ulrich, P. and Bouiflane, M. (2007), "Magnetic mapping for the detection and characterization of UXO: use of multi-sensor fluxgate 3-axis magnetometers and methods of interpretation", *Journal of Applied Geophysics*, Vol. 61, pp. 168-83.

Phillips, J.W., Leahy, R.M. and Mosher, J.C. (1997), "MEG based imaging of focal neuronal current sources", *IEEE Transactions on Medical Imaging*, Vol. 16 No. 3, pp. 338-48.

Schultze, V., Linzen, S., Schüler, T., Chwala, A., Stolz, R., Schulz, M. and Meyer, H.-G. (2008), "Rapid and sensitive magnetometer surveys of large areas using SQUIDs – the measurement system and its application to the Niederzimmern neolithic double-ring ditch exploration", *Archaeological Prospection*, Vol. 15, pp. 113-31.

Wang, J.Z., Williamson, S.J. and Kaufman, L. (1993), "Magnetic source images determined by a lead-field analysis: the unique minimum-norm least squares estimation", *IEEE Transactions on Biomedical Engineering*, Vol. 39 No. 7, pp. 665-75.

Corresponding author
Roland Eichardt can be contacted at: roland.eichardt@tu-ilmenau.de